Reaction $K^+p \to K^0\pi^+p$ at 2.26 BeV/c*

FREDERICK BOMSE, SAMUEL BORENSTEIN, JAMES COLE, DANIEL GILLESPIE, ROBERT KRAEMER, GEORGE LUSTE, IRVIN MILLER, EDWARD MOSES, AIHUD PEVSNER, RANDHIR SINGH, AND RICHARD ZDANIS

Department of Physics, The Johns Hopkins University, Baltimore, Maryland

(Received 7 November 1966)

The properties of the K^*(895 MeV) and N^*(1238 MeV) resonances produced in the reaction $K^+p \to K^0\pi^+p$ at 2.26 BeV/c are studied. The production of one or the other of these resonances is found to occur in this channel 80% of the time. The decay correlations of the K^* and N^* indicate that the dominant mechanism involved in their production may be single-vector-meson exchange. In particular, the decay angular distributions of the N^* are in good agreement with the predictions of the Stodolsky-Sakurai model. The experimental differential cross sections for production of each of these resonances are also compared with theoretical predictions based on a single-meson-exchange model which includes the effects of absorption due to competing channels. The agreement of the data with the theory is found to be only moderate here.

1. INTRODUCTION

THE Brookhaven National Laboratory 20-in. hydrogen bubble chamber was exposed to a beam of K^+ mesons. The laboratory momentum of the beam at the chamber entrance window was 2.260 BeV/c with a full width at half-maximum of 0.045 BeV/c. This momentum corresponds to a total center-of-mass energy for the K^+-proton system of (2.338±0.074) BeV.

There are several inelastic channels open in K^+-proton scattering at this energy. In particular, the three-particle final-state reaction $K^+p \to K^0\pi^+p$ is studied. Some of our results have been published.[1] This reaction is found to be dominated by two highly resonant channels:

$$K^+p \to K^{*+}p \to K^0\pi^+p,$$
$$K^+p \to N^{*++}K^0 \to K^0\pi^+p,$$

where K^{*+} is the 890-MeV K-π state and N^{*++} is the 1238-MeV isobar.

The shapes and positions of these resonances, as well as the cross sections for their production, are determined by analyzing the three-body Dalitz plot population for the reaction $K^+p \to K^0\pi^+p$. In addition, the experimental[2–11] production and decay angular distributions of the K^* and N^* are compared with theoretical predictions based on a single-particle-exchange model.[12–19] Both sets of distributions are consistent with the assumption that the predominant production mechanism is the exchange of a vector meson between the incoming particles.

2. EXPERIMENTAL METHOD

The raw data for this experiment consist of approximately 100 000 bubble chamber photographs, all of which were scanned for events with two charged prongs and an associated vee. A subset of 30 000 pictures was scanned twice to determine scanning efficiencies. These were typically on the order of 90%. All events with two positively charged prongs and an associated vee which had both production and vee vertices inside a specified fiducial volume were measured on a microscope in con-

* Supported in part by the National Science Foundation, the U. S. Air Force Office of Scientific Research Grant No. AFOSR 234-65, and the U. S. Atomic Energy Commission Computation Center.

[1] F. Bomse *et al.*, in *The Proceedings of the Second Topical Conference on Resonant Particles* (University of Ohio, Athens, Ohio, 1965).

[2] Brookhaven National Laboratory Bubble Chamber Group Internal Reports: T. W. Morris F-18 (1959), W. J. Willis F-28 (1960), J. K. Kopp F-55 (1961), F-49 (1961), F-62 (1962), F-68 (1962), F-67 (1960), and I. O. Skillicorn F-94 (1962) (all unpublished).

[3] M. G. Bowler, R. W. Bland, J. L. Brown, G. Goldhaber, J. A. Kadyk, F. Seeger, and G. H. Trilling, in *Proceedings of the Oxford International Conference on Elementary Particles, 1965*, Abstract A-92 (Rutherford High Energy Laboratory, Harwell, England, 1966).

[4] B. Kehoe, Phys. Rev. Letters **11**, 93 (1963).

[5] E. Boldt, J. Dubec, N. H. Duong, P. Eberhard, R. George, V. P. Henri, F. Levy, J. Poyen, M. Pripstein, J. Crussand, and A. Tran, Phys. Rev. **133**, B220 (1964).

[6] G. B. Chadwick, D. J. Crennell, W. T. Davies, M. Derrick, J. H. Mulvey, P. B. Jones, D. Radojicie, C. A. Wilkinson, A. Bettini, M. Cresti, S. Limentani, L. Peruzzo, and R. Santangelo, Phys. Letters **6**, 309 (1963).

[7] S. Goldhaber, W. Chinowsky, G. Goldhaber, and T. O'Halloran, Phys. Rev. **142**, 913 (1966).

[8] S. Goldhaber, J. L. Brown, I. Butterworth, G. Goldhaber, A. A. Hirata, J. A. Kadyk, and G. H. Trilling, Phys. Rev. Letters **15**, 737 (1965).

[9] M. Ferro-Luzzi, R. George, Y. Goldschmidt-Clermont, V. P. Henri, B. Jongejans, D. W. Leith, G. R. Lynch, F. Muller, and J. M. Perreau, Nuovo Cimento **36**, 1105 (1965).

[10] P. Sallstrom, G. Otber, and G. Ekspong, in *Proceedings of the Oxford International Conference on Elementary Particles, 1965*, Abstract A-135 (Rutherford High Energy Laboratory, Harwell, England, 1966).

[11] R. George, Y. Goldschmidt-Clermont, V. P. Henri, B. Jongejans, W. Koch, D. W. Leith, G. Lynch, A. Moisseev, F. Muller, J. M. Perreau, and V. Iarba, in *Proceedings of the Oxford International Conference on Elementary Particles, 1965*, Abstract A-129 (Rutherford High Energy Laboratory, Harwell, England, 1966).

[12] J. D. Jackson, Nuovo Cimento **34**, 1644 (1964).

[13] J. D. Jackson and H. Pilkuhn, Nuovo Cimento **33**, 906 (1964).

[14] B. E. Y. Svennson, Nuovo Cimento **37**, 714 (1965).

[15] K. Gottfried and J. D. Jackson, Nuovo Cimento **33**, 309 (1964).

[16] K. Gottfried and J. D. Jackson, Nuovo Cimento **34**, 735 (1964).

[17] J. D. Jackson, Rev. Mod. Phys. **37**, 484 (1965).

[18] J. D. Jackson, J. T. Donohue, K. Gottfried, R. Keyser, and B. E. Y. Svennson, Phys. Rev. **139**, B428 (1965).

[19] L. Stodolsky and J. J. Sakurai, Phys. Rev. Letters **11**, 90 (1963).

junction with a digitized Brower film stage. The estimated error in a measured coordinate was about 2 μ on the film. The results of these measurements were used as input to the Brookhaven analysis programs TRED and KICK[1] which performed, respectively, stereo reconstruction and kinematic fitting of the events. All computing was done on an IBM 7094.

After fitting, the events were examined by a physicist on a scanning table to compare observed track ionizations with those of the kinematic fits. In this way, 95% of the events in this topology were assigned unambiguous interpretations. In particular, there were 709 events of the type $K^+p \to K^0\pi^+p$ in which the K^0 was identified by a visible vee. The resolution of the experiment was estimated by refitting a sample of these events with the vee vertex translated to coincide with the production vertex and all information on the K^0 deleted. This procedure enabled one to calculate an experimental mass and width for the K^0 from the decay pions, without requiring their effective mass to be 497 MeV. This is contrary to the technique employed by KICK in fitting the vee, in which the two decay tracks are forced to have an effective mass corresponding to the K^0. The effective mass squared of the $\pi^+\pi^-$ combination was calculated for each event and the resulting distribution when fitted with a Gaussian, peaked at 0.247 BeV^2 with a full width at half-maximum of 0.008 BeV^2. This corresponds to a K^0 mass of 497 MeV and a resolution in fitted mass of about 10 MeV.

3. CROSS SECTIONS AND DALITZ PLOT ANALYSIS

The total cross section for the reaction $K^+p \to K^0\pi^+p$ is determined from the total length of beam track and the number of observed reactions of this type within a specified fiducial volume. The total length of beam track in 30 000 doubly scanned pictures measured inside the fiducial volume had to be corrected before use to account for π and μ contamination in the beam. This contamination was found by comparing the number of τ and τ-like decays observed, with the number of these expected for an absolutely pure K^+ beam. The comparison yielded a result of (20±3)% for the beam contamination. The number of reactions observed in the experiment had to be corrected to account for: (a) scanning efficiency; (b) K^0 mesons which decayed either outside the fiducial volume or within 2 mm of the production vertex. (The latter restriction is imposed in order to eliminate the difficulty in distinguishing the two-prong-plus-vee topology from the four-prong topology when the vee occurred too near the production vertex.) (c) K^0 mesons which did not decay into two charged mesons.

With these corrections the total beam length was found to be 11.49×10^6 cm and the number of observed reactions was 1128. These results yielded a total cross section: $\sigma(K^+p \to K^0\pi^+p) = (2.62\pm0.30)$ mb. This result is compared with those of other experiments in

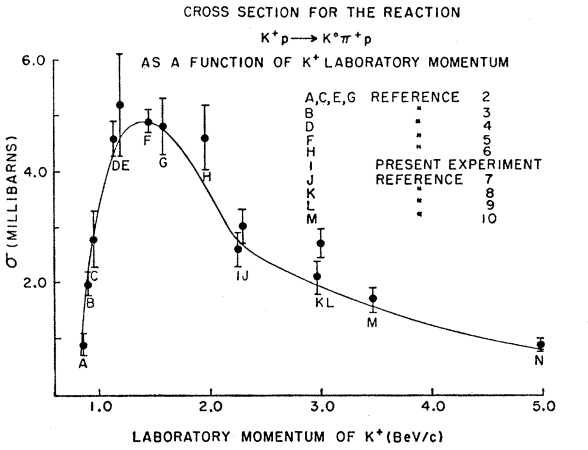

FIG. 1. Cross section for the reaction $K^+p \to K^0\pi^+p$ as a function of incoming K^+ laboratory momentum.

Fig. 1. The solid curve in the figure is a free-hand fit to the experimental points. We remark that the cross section for this reaction is about 1.0 mb near threshold, increases to about 5.0 mb at a laboratory K^+ momentum of 1.5 BeV/c, and then decreases to 1.0 mb over a range of K^+ momenta from 1.5–5.0 BeV/c.

The cross sections for the production of the K^* and N^* resonances were obtained by analyzing the population of the three-body Dalitz plot for this reaction which is shown in Fig. 2. We assumed that this plot could be interpreted in terms of three noninterfering amplitudes: $A_{K^*}(M_{K\pi}{}^2, M_{p\pi}{}^2)$, $A_{N^*}(M_{K\pi}{}^2, M_{p\pi}{}^2)$ and A_B where

$A_{K^*}(M_{K\pi}{}^2, M_{p\pi}{}^2)$ = amplitude for $K^+p \to K^{*+}p$,

$A_{N^*}(M_{K\pi}{}^2, M_{p\pi}{}^2)$ = amplitude for $K^+p \to N^{*++}K^0$,

A_B = amplitude for $K^+p \to K^0\pi^+p$,

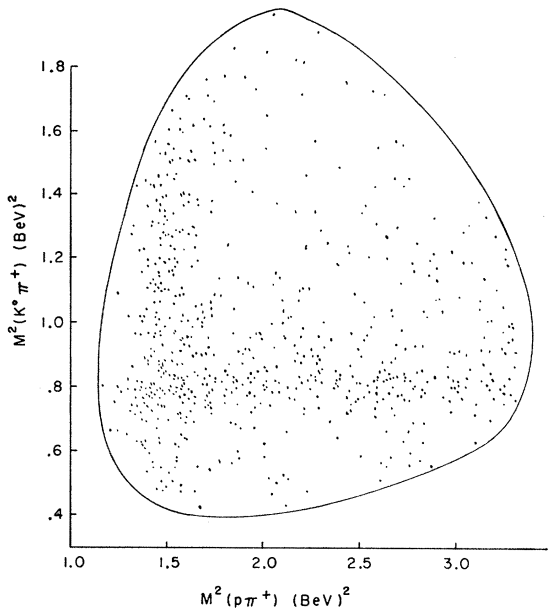

FIG. 2. Dalitz plot for the reaction $K^+p \to K^0\pi^+p$ at 2.26 BeV/c.

with no correlations whatever among the three final-state particles. Thus the number of events having K-π effective mass squared between $M_{K\pi}{}^2$ and $M_{K\pi}{}^2+dM_{K\pi}{}^2$ and p-π effective mass squared between $M_{p\pi}{}^2$ and $M_{p\pi}{}^2+dM_{p\pi}{}^2$, $(\partial^2 N/\partial M_{K\pi}{}^2)\partial M_{p\pi}{}^2$ is

$$\frac{\partial^2 N}{\partial M_{K\pi}{}^2 \partial M_{p\pi}{}^2} = |A_{K^*}(M_{K\pi}{}^2, M_{p\pi}{}^2)|^2 + |A_{N^*}(M_{K\pi}{}^2, M_{p\pi}{}^2)|^2 + |A_B|^2. \quad (1)$$

Jackson[12] has discussed appropriate forms for resonance terms like $|A_{K^*}|^2$ and $|A_{N^*}|^2$. Following the general ideas outlined in Ref. 11, we take the explicit expressions for the absolute squares of the resonance amplitudes to be

$$|A_{K^*}|^2 = \left[\frac{\Gamma(M_{K\pi})}{(M_{K^*}{}^2 - M_{K\pi}{}^2)^2 + \Gamma^2(M_{K\pi}) M_{K^*}{}^2}\right] \times \left(\frac{M_{K\pi} P_p{}^2}{q_K}\right), \quad (2)$$

$$\Gamma(M_{K\pi}) = \left(\frac{q_K}{q_K{}^0}\right)^3 \frac{M_{K^*}}{M_{K\pi}} \Gamma_{K^*}, \quad (3)$$

where M_{K^*}, Γ_{K^*} are the intrinsic mass and width of the K^*, P_p is the proton momentum in the over-all center-of-mass system, q_K is the momentum of the K^0 in the K^* rest frame, and $q_K{}^0$ is the value of q_K for $M_{K\pi}=M_{K^*}$.

$$|A_{N^*}|^2 = \left[\frac{\Gamma(M_{\pi p})}{(M_{N^*}{}^2 - M_{p\pi}{}^2)^2 + \Gamma^2(M_{p\pi}) M_{N^*}{}^2}\right] \times \left(\frac{M_{p\pi} P_K{}^2}{q_p}\right), \quad (4)$$

$$\Gamma(M_{p\pi}) = \left(\frac{q_p}{q_p{}^0}\right)^3 \left[\frac{(M_{p\pi}+M_p)^2 - M_\pi{}^2}{M_{p\pi}{}^2}\right] \times \left[\frac{M_{N^*}{}^2}{(M_{N^*}+M_p)^2 - M_\pi{}^2}\right] \Gamma_{N^*}, \quad (5)$$

where M_{N^*}, Γ_{N^*} are the intrinsic mass and width of the N^*, P_K is the K^0 momentum in the over-all center-of-mass system, q_p is the momentum of the proton in the N^* rest frame, and $q_p{}^0$ is the value of q_p for $M_{p\pi}=M_{N^*}$. The resonance amplitudes squared in these formulas are expressed[11] in terms of resonant phase shifts:

$$|A|^2 \sim \frac{\sin^2\delta}{M_0 \Gamma(M)}, \quad (6)$$

$$\tan\delta = \frac{M_0 \Gamma(M)}{M_0{}^2 - M^2}, \quad (7)$$

where δ, the phase shift at resonance defined in (7), is related to the relativistic Breit-Wigner shapes (2) and (4), through (6). In (6) and (7), M_0 may be M_{K^*} or M_{N^*}, and M, may be either $M_{K\pi}$ or $M_{p\pi}$. In Eqs. (2) and (4), the second factor in brackets is a phase-space factor. Ordinarily, one would write merely $(M_{K\pi}/q_K)$. Integration over the $M_{p\pi}{}^2$ axis of the Dalitz plot would then result in an over-all factor of P_p. However, for the case of K^* production by exchange of a vector meson (which we anticipate here), an over-all factor of $P_p{}^3$ is more appropriate.[12] Thus the usual phase-space factor is modified by $P_p{}^2$. The expressions (3) and (5) give the mass variations of the widths $\Gamma(M_{K\pi})$ and $\Gamma(M_{p\pi})$. They are of the form[12]

$$\Gamma = \Gamma_0 \left(\frac{q}{q_0}\right)^{2l+1} \frac{\rho(M)}{\rho(M_0)}, \quad (8)$$

where q, M, Γ, q_0, M_0, and Γ_0 are defined above and l is the relative orbital angular momentum of the decay products. Equation (3) is then appropriate to the decay of a 1^- meson into two pseudoscalar bosons and (5), to the decay of a $\frac{3}{2}^+$ baryon into a pseudoscalar boson and a spin-$\frac{1}{2}$ fermion. We note in connection with the resonance amplitudes, Jackson's comment[12] that the mass-dependent width $\Gamma(M)$ can, for a broad resonance near threshold, cause considerable distortion of the shape, with the peak falling below M_0. We expect this effect to be noticeable in our N^* data, for the N^* is quite near the lower limit of phase space and is known to be a fairly broad resonance. In Eqs. (2) and (4) we note the dependence of the amplitudes and their squares on one of the masses only. For example we have $A_{K^*}=A_{K^*}(M_{K\pi})$ with no dependence on $M_{p\pi}$. This is tantamount to the simplifying assumption made in fitting the data that each of the resonances decays isotropically in its rest

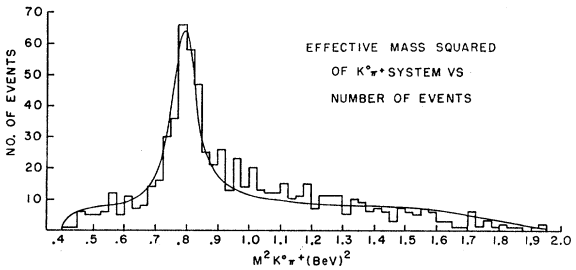

FIG. 3. Projection of the Dalitz plot on the $M_{K\pi}{}^2$ axis.

TABLE I. Masses and widths of the K^* and N^*, and fractions of production.

	This work 2.26 BeV/c	Reference 9 2.97 BeV/c
M_{K^*}	895±3 MeV	891±3 MeV
Γ_{K^*}	50±5 MeV	47±4 MeV
Fraction K^*	(42±3)%	(38±3)%
M_{N^*}	1234±5 MeV	1232±6 MeV
Γ_{N^*}	120±20 MeV	125±30 MeV
Fraction N^*	(40±3)%	(38±3)%

frame. Finally A_B, the amplitude for $K^+p \to K^0\pi^+p$ with no correlations among the final-state particles, is taken to be a constant in accordance with the fact that a three-body Dalitz plot is populated uniformly by Lorentz-invariant phase-space events.

We compare our data with the theory outlined above by performing least-squares fits to the projections of the Dalitz plot on the $M_{K\pi}^2$ and $M_{p\pi}^2$ axes. It is therefore necessary to integrate the functions $|A_{K^*}|^2$, $|A_{N^*}|^2$, $|A_B|^2$ over one or the other of these axes. The procedure followed in fitting, say the $M_{K\pi}^2$ projection, is as follows. First we define three functions:

$$f_1(M_{K\pi}) = \int |A_{K^*}|^2 dM_{p\pi}^2,$$

$$f_2(M_{K\pi}) = \int |A_{N^*}|^2 dM_{p\pi}^2,$$

$$f_3(M_{K\pi}) = \int |A_B|^2 dM_{p\pi}^2.$$

These functions are normalized so that we have

$$\int f_1 dM_{K\pi}^2 = \int f_2 dM_{K\pi}^2 = \int f_3 dM_{K\pi}^2 = 1.$$

We then note that $f_2(M_{K\pi})$ and $f_3(M_{K\pi})$ have the same general shape, so that the fitting technique is incapable of making a sharp distinction between them. Thus, an attempted fit results in an almost singular error matrix. We circumvent this problem by fitting the $M_{K\pi}^2$ projection to a form: $\alpha f_1(M_{K\pi}) + \beta[f_2(M_{K\pi}) + f_3(M_{K\pi})]$, where α represents the fraction of events which proceed only by $K^+p \to K^*p$ and β, the fraction which proceeds by either of the processes $K^+p \to N^*K$ or $K^+p \to K^0\pi^+p$. This fit produces a unique result for α. By following a similar procedure for the $M_{p\pi}^2$ projection, the fraction of events α', which proceeds only by the channel $K^+p \to N^*K$ is determined. Finally, we find the fraction of events which proceeds according to a constant matrix element, α'', by imposing the constraint on the two fits that $\alpha+\alpha'+\alpha''=1$, a legitimate step in view of our assumption of noninterference of the amplitudes. As a check on this assumption, we find that according to the fit we expect about 40 N^* events within the K^* mass band (0.71–0.88) BeV^2 and about 55 K^* events are expected in the N^* mass band (1.28–1.69) BeV^2. Furthermore there should be, according to these fits about 4 phase-space events in the N^*-K^* overlap region. Thus our fits predict about 99 events altogether in the N^*-K^* overlap box in excellent agreement with the experimental number, 95±10. In addition, the best values of the intrinsic masses and widths are determined from these fits. For the K^*, the results are: $M_{K^*}=895\pm3$ MeV, $\Gamma_{K^*}=50\pm5$ MeV with (42±3)% of the sample proceeding by the channel $K^+p \to K^*p$. We find for the N^*: $M_{N^*}=(1234\pm5)$ MeV, $\Gamma_{N^*}=120\pm20$ MeV with (40±3)% of the events proceeding by the channel $K^+p \to N^*K$. These results are tabulated and compared with those of the CERN group[9] in Table I. The form of the amplitudes used to fit the three-body Dalitz plot in their experiment are the same as those used here. The results for the K^* and N^* parameters are in good agreement. The projections of the Dalitz plot on the $M_{K\pi}^2$ and $M_{p\pi}^2$ axes are shown in Figs. 3 and 4. In each case the histogram indicates the experimental data and the solid curve is the least-squares solution. As expected,[12] the experimental peak of the N^* (Fig. 4) is shifted downward occurring at a value of $M_{p\pi}$ of 1215 MeV in comparison with the intrinsic mass of 1234 MeV. From the fractions of events in each resonant channel we find the partial cross sections to be

$$\sigma(K^+p \to K^*p \to K^0\pi^+p) = (1.1\pm0.2) \text{ mb},$$
$$\sigma(K^+p \to N^*K \to K^0\pi^+p) + (1.1\pm0.2) \text{ mb}.$$

These results are compared with other experiments in Figs. 5 and 6. As before, the solid curves in these figures are free hand fits to the experimental points.

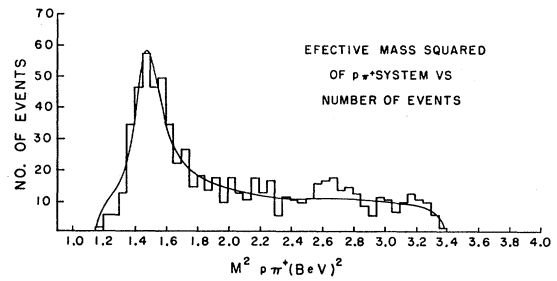

FIG. 4. Projection of the Dalitz plot on the $M_{p\pi}^2$ axis.

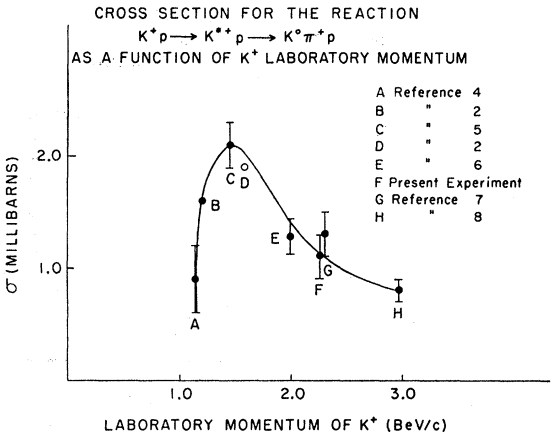

FIG. 5. Cross section for the reaction $K^+p \to K^{*+}p$ as a function of incoming K^+ laboratory momentum.

4. DECAY CORRELATIONS OF THE RESONANCES

Figures 12 and 13 show the experimental production differential cross sections as a function of center-of-mass production angle of the K^* and N^*, respectively. The forward or backward peaking of these cross sections is

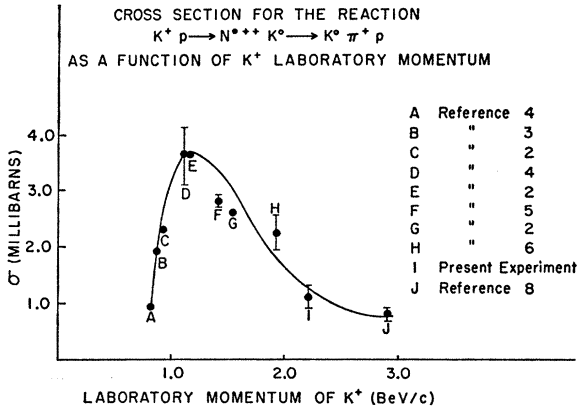

FIG. 6. Cross section for the reaction $K^+p \to N^{*++}K^0$ as a function of incoming K^+ laboratory momentum.

accepted as evidence that the reactions $K^+p \to K^*p$ and $K^+p \to N^*K$ are mediated by a single-particle-exchange mechanism and the data are therefore compared with theoretical predictions based on a peripheral or single-particle-exchange model. Models of this type are widely discussed in the literature.[12–19]

The structure of the decay angular distributions often indicates[17,18] that the production of resonances is consistent with the exchange of an object of given spin and parity. The angular distributions of the K^* and N^* in in this experiment are analyzed accordingly. A convenient coordinate system in which to observe these distributions has been suggested by Jackson and

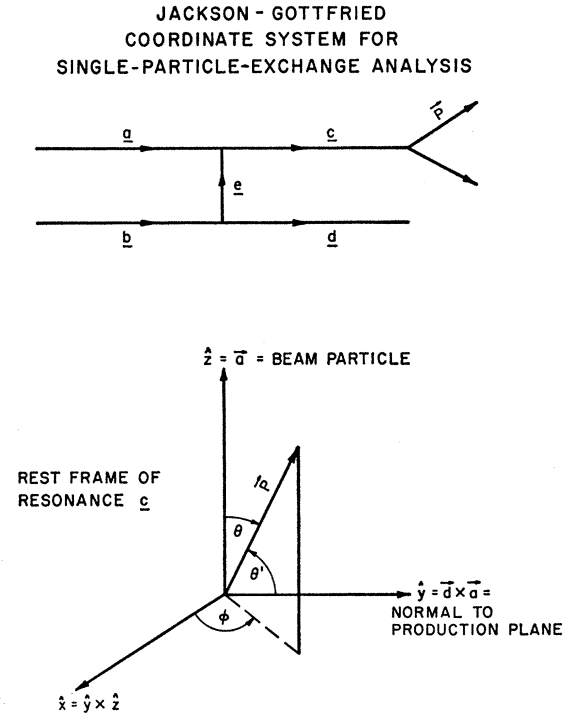

FIG. 7. Coordinate system for analyzing decay correlations of the resonances.

Gottfried[15] and is shown in Fig. 7. This system, defined in the rest frame of the resonance, has its z axis along the direction of the incoming particle (particle A in the upper part of Fig. 6). The y axis is along the normal to the production plane defined by $\mathbf{d}\times\mathbf{a}=\mathbf{a}\times\mathbf{c}$ where $\mathbf{d}, \mathbf{a}, \mathbf{c}$ refer to three-momenta of the respective particles in this figure. Finally, the x axis is in the direction of the cross product of y with z. Relative to this system, the polar and azimuthal angles (θ,ϕ) of the three-momentum vector of a resonance decay product are defined in the conventional manner. The angle θ' between this vector and the production normal is also shown. In terms of (θ,ϕ) the decay angular distributions for $K^* \to K^0\pi^+$ and $N^* \to p\pi^+$ are, respectively,[12,15]

$$W_{K^*}(\cos\theta,\phi) = \frac{3}{4\pi}\left[\rho_{00}\cos^2\theta+\tfrac{1}{2}(1-\rho_{00})\sin^2\theta-\rho_{1-1}\sin^2\theta\cos2\phi - \sqrt{2}\,\mathrm{Re}\rho_{10}\sin2\theta\cos\phi\right], \quad (9)$$

$$W_{N^*}(\cos\theta,\phi) = \frac{3}{4\pi}\rho_{33}\sin^2\theta+(\tfrac{1}{2}-\rho_{33})\tfrac{1}{3}+\cos^2\theta - \frac{2}{\sqrt{3}}\mathrm{Re}\rho_{31}\sin2\theta\cos\phi-\frac{2}{\sqrt{3}}\mathrm{Re}\rho_{3,-1}\sin^2\theta\cos2\phi, \quad (10)$$

where the ρ_{ij} are the spin-space density matrix elements of the K^* or N^* and W_{K^*} and W_{N^*} are normalized to unity. Equation (9) is simply obtained by realizing that in the decay $K^* \to K^0\pi^+$, angular momentum and parity conservation require the decay products to be in a relative P state. Thus their wave function is of the form

$$\Psi \sim A_1Y^1(\theta,\phi)+A_0Y_1{}^0(\theta,\phi)+A_{-1}Y_1{}^{-1}(\theta,\phi),$$

where $Y_1{}^m$ is a spherical harmonic of order 1. Then

$$W(\theta,\phi)\sim\Psi^*\Psi=\textstyle\sum_{m,n}(A_n{}^*A_m)Y_1{}^{n*}Y_1{}^m$$

and (9) follows upon identifying ρ_{nm} with $A_m{}^*A_n$ and carrying out the indicated expansion. The normalization of the distribution also requires that Tr $\rho=1$. Equation (10) is similarly obtained. The decay $N^* \to p\pi^+$ must also occur in a P state. However in this case, the proton spin state must be included in the wave function. Stodolsky and Sakurai[19] have suggested that the N^* decay distribution could be more conveniently expressed in terms of the angle θ' (Fig. 7). This may be obtained by rotating (10) to a coordinate system in which the z axis is along the production normal, and integrating over an azimuthal angle. The result is

$$W_{N^*}(\cos\theta') = \frac{3}{4\pi}\left[\frac{\rho_{33}'+\rho_{-3-3}'}{2}\sin^2\theta' + \frac{\rho_{11}'+\rho_{-1-1}'}{2}\left(\frac{1+3\cos^2\theta'}{3}\right)\right]. \quad (11)$$

The ρ' here are the N^* density matrix elements in the rotated coordinate system and are related to the ρ of (10) by simple algebraic expressions. The angle ϕ in the distributions (9), (10) is the familiar Treiman-Yang angle.[12]

In general, the values of the density matrix elements are not predicted by the theory, but the experimental values obtained are indicative of the nature of the exchanged particle. However, the Stodolsky-Sakurai model[19] for N^* production (in which pseudoscalar exchange is not allowed) by ρ meson exchange does make definite predictions about the values of the primed density matrix elements of Eq. (11). This model requires that $\rho_{33}'+\rho_{-3-3}'=0$. Hence the distribution in $\cos\theta'$ for the N^* decay products should be $W_{N^*}(\cos\theta') \sim (1+3\cos^2\theta')$. Furthermore, on transforming back to the coordinate system in which θ is the polar angle, rather than θ' (Fig. 7), one finds that $\rho_{33}'+\rho_{-3-3}'=0$ implies that $\rho_{33}=\frac{3}{8}$ and $\mathrm{Re}\rho_{3-1}=\frac{3}{8}$. Upon integrating (10) over θ, the N^* Treiman-Yang distribution becomes $W_{N^*}(\phi)=\frac{1}{2}(1+2\sin^2\phi)$. We summarize the predictions about the N^* angular distributions based on Stodolsky and Sakurai's model as follows:

$$W_{N^*}(\cos\theta') \sim (1+3\cos^2\theta'), \quad W_{N^*}(\phi) \sim (1+2\sin^2\phi), \tag{12}$$

where θ', ϕ are discussed above and indicated in Fig. 7.

Although specific predictions analogous to the above are not made about the K^* density matrix elements it is easy to see how the nature of the exchanged object determines their values and correspondingly the structure of the angular distribution (9). If, for example, the reaction $K^+p \to K^*p$ proceeds by pseudoscalar meson exchange, two pseudoscalars (the beam K^+ and the exchanged pseudoscalar) must combine at the upper vertex of Fig. 7 to produce a 1^-K^*. This can only occur in an $l=1$, $m_l=0$ configuration. Hence the K^* must have total-angular-momentum quantum numbers $J=1$, $M=0$. The decay wave function is then: $\Psi \sim Y_1^0$ and the decay distribution is of the form: $W \sim |Y_1^0|^2=\cos^2\theta$. This implies that $\rho_{00}=1$ and all other density matrix elements are zero. On the other hand if vector meson exchange is responsible for this reaction then the K^* must be formed from the incident K^+, a 0^- object, and the exchanged 1^- meson. This can only happen when the K^* spin has a projection on the z axis (Fig. 7) of ± 1. The decay wave function is then, $\Psi \sim Y_1^1+Y_1^{-1}$, and the angular distribution W is proportional to $|Y_1^1+Y_1^{-1}|^2 \sim [\frac{1}{2}\sin^2\theta-\frac{1}{2}\sin^2\theta\cos 2\phi]$. One then has $\rho_{00}=0$ and $\rho_{11}=\frac{1}{2}(1-\rho_{00})=\frac{1}{2}$. Also the element ρ_{1-1} has its maximum value of $\frac{1}{2}$. The presence of the $\cos 2\theta$ term in the above is due to interference between the Y_1^1 and Y_1^{-1} components of the wave function, which arises because the K^* spin direction, or equivalently, the spin direction of the exchanged particle is not detected. Jackson and Pilkuhn[13] have pointed out that in the absence of any absorptive correction to the peripheral model, the pseudoscalar and vector meson exchange processes, if they both occur, must be incoherent. The decay distribution then has the general form $W \sim |Y_1^0|^2 + |Y_1^1+Y_1^{-1}|^2$. This implies that $\mathrm{Re}\rho_{10}$ in (9) is zero. In this case ρ_{00} represents the fraction of events which is mediated by pseudoscalar exchange. To recapitulate then, an experimentally determined value of ρ_{00} which is close to 1 indicates predominantly pseudoscalar meson exchange and a distribution which is mostly $\cos^2\theta$. Alternatively, a value of ρ_{00} near zero and a predominantly $\sin^2\theta$ distribution indicates a large amount of vector relative to pseudoscalar exchange. In this case the value of ρ_{1-1} is indicative of the interference between the exchanged meson's polarization states which results in the azimuthal or Treiman-Yang anisotropy in the decay angular distribution. Finally, a nonzero value of $\mathrm{Re}\rho_{10}$ may indicate that the simple peripheral model needs modification. We return to this point later.

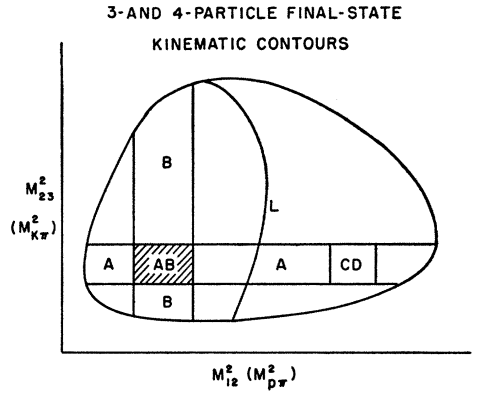

FIG. 8. Schematic diagram of Dalitz contour and resonance bands.

To calculate the density matrix elements of the resonances, we select events within specified mass intervals. We define the K^* band as the interval on the $M_{K\pi}{}^2$ axis of the Dalitz plot between 0.71 and 0.88 BeV^2, and the N^* band as the interval between 1.28 and 1.69 BeV^2 on the $M_{p\pi}{}^2$ axis. To avoid biases which could occur in these calculations because of the overlapping of the resonance bands, we calculate the density matrix elements for three different samples of events. These are most easily described with reference to Fig. 8 which is a schematic diagram of the Dalitz contour and the resonance bands. Sample 1, for each resonance consists of all the events in the resonance band including those in the overlap region AB. Thus in Sample 1, the events in AB are assigned to both the K^* and N^* bands. Sample 2 in each case consists of all events in the band excluding the overlap region entirely. In choosing Sample 3 events we follow a suggestion of Eberhard and Pripstein.[20] A region CD is found in each of the resonance bands whose population by resonance events is theoretically

[20] P. Eberhard and M. Pripstein, Phys. Rev. Letters **10**, 351 (1963).

TABLE II. Density matrix elements obtained from the various samples of events. The lower part of the table shows the results of dividing Sample 3 into halves as a check.

Element	Sample 1	Sample 2	Sample 3	Stodolsky-Sakurai
ρ_{00}	0.15 ±0.04	0.15±0.04	0.15±0.05	···
$\rho_{1,-1}$	0.13 ±0.04	0.30±0.05	0.24±0.04	···
$\mathrm{Re}\rho_{10}$	−0.07 ±0.02	−0.04±0.03	−0.05±0.03	···
ρ_{33}	0.28 ±0.03	0.27±0.04	0.28±0.03	0.375
$\mathrm{Re}\rho_{3,-1}$	0.24 ±0.03	0.19±0.04	0.21±0.03	0.216
$\mathrm{Re}\rho_{31}$	−0.006±0.03	−0.03±0.04	−0.03±0.03	···
	$M_{K\pi}{}^2$=0.71–0.79 BeV²	$M_{K\pi}{}^2$=0.79–0.88 BeV²	$M_{p\pi}{}^2$=1.28–1.48 BeV²	$M_{p\pi}{}^2$=1.48–1.69 BeV²
ρ_{00}	0.15 ±0.07	0.13±0.06		
$\rho_{1,-1}$	0.13 ±0.07	0.30±0.06		
$\mathrm{Re}\rho_{10}$	−0.006±0.04	−0.09±0.03		
ρ_{33}			0.27±0.05	0.30 ±0.04
$\mathrm{Re}\rho_{3,-1}$			0.22±0.04	0.21 ±0.04
$\mathrm{Re}\rho_{31}$			−0.06±0.05	−0.007±0.04

equal to the population of overlap region AB by events belonging to the same resonance. These two regions are conjugate to each other in the sense that events in CD are parity inversions of events in AB. Parity inversion here implies that in the resonance rest frame, the decay 3-momenta are exchanged. Assuming that the resonance decays as a free particle in a given parity state, conservation of parity requires equal population of the conjugate regions.[20] Sample 3 is then constructed for each resonance as follows. An appropriate region CD is found and the experimental events inside this region are used to construct a set of fictitious events which are parity inversions of them. The experimental events in AB are then removed and this region is repopulated with the fictitious events. These, plus the remainder of the band comprise Sample 3. Events in Sample 3 are assumed to be a good approximation to the structure of one resonance band when the other is absent.

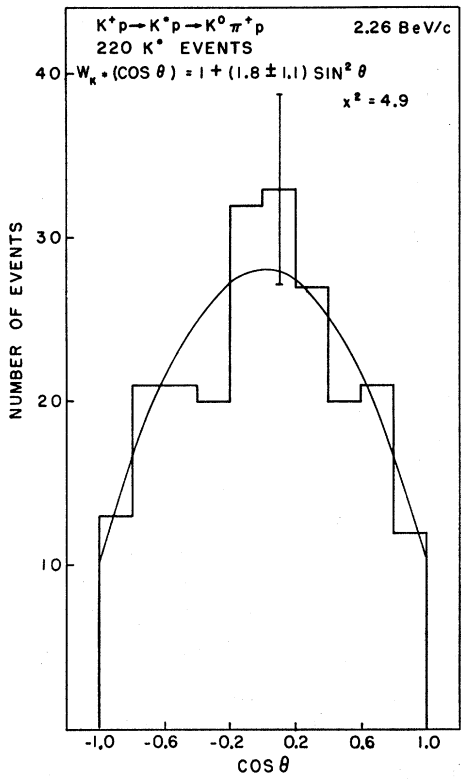

FIG. 9. Cosθ distribution for the decay $K^* \to K^0\pi^+$.

For each of the three samples, the density matrix elements are calculated by a moment analysis of the events. Denoting the average value of a function $f(\theta,\phi)$ over the experimental distribution by $\langle f\rangle$, we have

$$\langle f\rangle=\frac{1}{N}\sum_{i=1}^{N} f_i$$

where N is the total number of events and f_i is the value of $f(\theta,\phi)$ for the ith event. We assign an error[21]

$$\Delta\langle f\rangle=\frac{1}{N}[\sum_{i=1}^{N}(\langle f\rangle-f_i)^2]^{1/2}.$$

A little algebra shows that the angular distributions (9) and (10) can be expressed as linear combinations of spherical harmonics of order 2. If these are denoted by $Y_2{}^m$, we find that the density matrices can be expressed as follows:

$$K^*: \quad \rho_{00}=\tfrac{1}{3}(1+\tfrac{5}{2}\langle Y_2{}^0\rangle),$$

$$\rho_{1-1}=-\frac{5}{4}\langle \mathrm{Re}Y_2{}^2\rangle,$$

$$\mathrm{Re}\rho_{10}=\frac{-5}{4\sqrt{2}}\langle \mathrm{Re}Y_2{}^1\rangle.$$

$$N^*: \quad \rho_{33}=\tfrac{1}{4}[1-\tfrac{5}{2}\langle Y_2{}^0\rangle],$$

$$\mathrm{Re}\rho_{3-1}=-\tfrac{5}{8}\sqrt{3}\langle \mathrm{Re}Y_2{}^2\rangle,$$

$$\mathrm{Re}\rho_{31}=-\tfrac{5}{8}\sqrt{3}\langle \mathrm{Re}Y_2{}^1\rangle.$$

[21] P. E. Schlein, D. D. Carmony, G. M. Perreau, W. E. Slater, D. H. Stork, and H. K. Ticho, Phys. Rev. Letters **11**, 167 (1963).

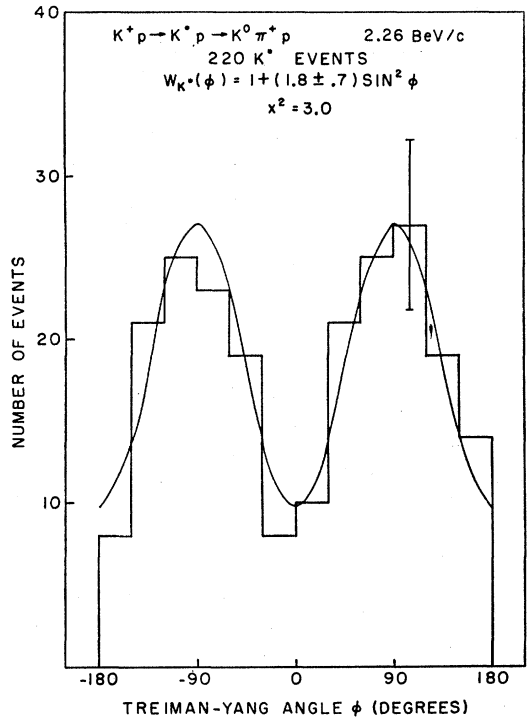

FIG. 10. Treiman-Yang distribution for the decay $K^* \to K^0\pi^+$.

The experimental values of the density matrix elements for each sample of events and for each resonance are listed in Table II. We note that the element ρ_{1-1} in the K^* density matrix appears quite sensitive to the way in which the resonance overlap region is handled. The remaining elements of the density matrices do not seem to vary much from sample to sample. As an additional check, each resonance band in Sample 3 is divided in half and the density matrix is calculated separately for events in each half. The results are shown in the bottom part of Table II. Interestingly enough the element ρ_{1-1} in the K^* density matrix again shows a fairly sharp variation from one half of the resonance to the other. Finally, we estimate the number of background or phase space events in each of the resonance bands, and assuming that these events would be isotropically distributed in every angle, recalculate the density matrices. The differences between these recalculated values and the values given in Table II were in all cases small and within the statistical errors. We have not therefore, attempted to correct the values in Table II to account for these small deviations. We remark, however, that we assume no interference effects between the resonant and background events and that such effects could possibly account for the differences between the values of ρ_{1-1} calculated for the separate halves of the K^*.

In discussing the results of the moment analysis and presenting the experimental angular distributions, we shall from now on restrict ourselves to Sample 3 events. Turning first to the K^* we show in Figs. 9 and 10 the $\cos\theta$ and ϕ angular distributions. These are of the form

$$W_{K^*}(\cos\theta) \sim [(1-\rho_{00})+(3\rho_{00}-1)\cos^2\theta], \quad (13)$$

$$W_{K^*}(\phi) \sim [(1-2\rho_{1,-1})+4\rho_{1,-1}\sin^2\phi]. \quad (14)$$

Substituting the experimental values of the density matrix elements in (13) and (14) and normalizing to the total number of events, we obtain the solid curves of Figs. 9 and 10. Aside from the normalization factor, the $\cos\theta$ distribution is given by: $W_{K^*}(\cos\theta) = 1+(1.8\pm1.1)\sin^2\theta$ with a value of ρ_{00} of 0.15 ± 0.05. Recalling that a low value of this element indicates predominantly vector meson exchange and a $\sin^2\theta$ distribution, we conclude that the distribution is consistent with vector exchange in K^* production. This is corroborated by considering the Treiman-Yang distribution for K^* events. According to (14) this distribution is characterized by the density matrix element ρ_{1-1}. This element is a measure of the departure of the Treiman-Yang angular distribution from isotropy. If, indeed, vector meson exchange predominates for K^* production in $K^+p \to K^*p$ as suggested by Fig. 9, then the Treiman-Yang distribution should show a $\sin^2\phi$ variation. A glance at Fig. 10 shows that this is the case. A value of ρ_{1-1} of 0.24 ± 0.04 leads to a distribution $W_{K^*}(\phi) = 1+(1.8\pm0.7)\sin^2\phi$. This distribution, normalized to the total number of K^* events, is shown as the solid curve in Fig. 10. The off-diagonal density matrix element $\mathrm{Re}\rho_{10}$ is -0.05 ± 0.03. The inconsistency of this result with the value zero, predicted by the simple

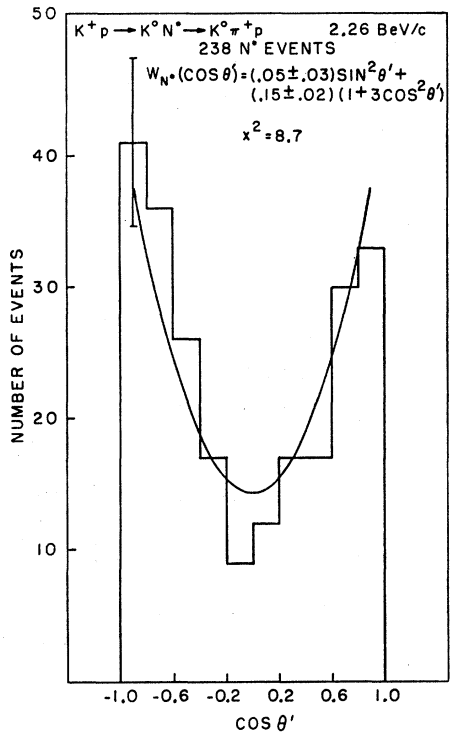

FIG. 11. $\cos\theta'$ distribution for the decay $N^* \to p\pi^+$.

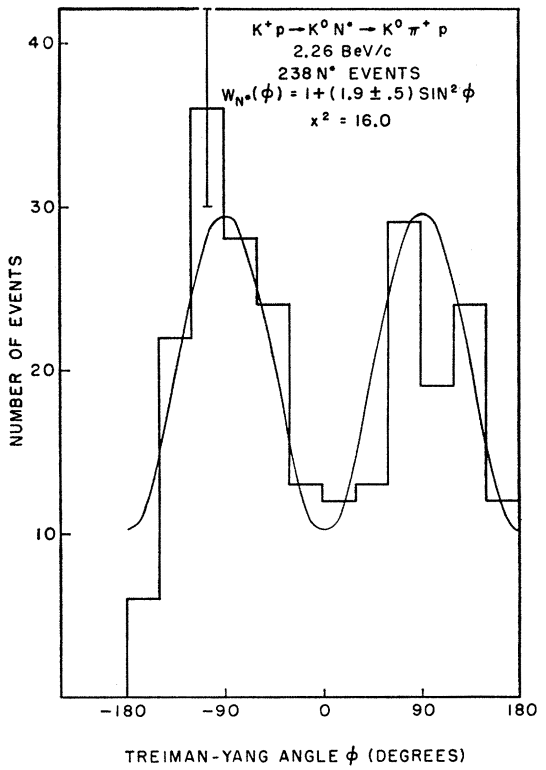

FIG. 12. Treiman-Yang distribution for the decay $N^* \to p\pi^+$.

peripheral model is in accordance with absorptive modifications introduced by Jackson and Gottfried.[16–18]

Figure 11 and 12 show the experimental angular distributions in $\cos\theta'$ and ϕ for N^* events from the channel $K^+p \to N^*K$. We recall that the $\cos\theta'$ distribution has the general form of Eq. (11) and that Stodolsky and Sakurai predict $\rho_{33}'+\rho_{-3-3}'=0$ and thus a distribution of the form $W_{N^*}(\cos\theta')\sim 1+3\cos^2\theta'$. When the experimental values of the N^* density matrix elements from Table II are used to calculate the primed elements, the results are

$$\tfrac{1}{2}(\rho_{11}'+\rho_{-1-1}')=0.45\pm0.06$$

and

$$\rho_{33}'+\rho_{-3,-3}'=0.05\pm0.03.$$

These numbers lead to a $\cos\theta'$ distribution which is:

$$W_{N^*}(\cos\theta')=(0.05\pm0.03)\sin^2\theta' + (0.15\pm0.02)(1+3\cos^2\theta').$$

It is normalized to the total number of N^* events and shown as the solid curve in Fig. 11. This result is in fairly good agreement with the pure $1+3\cos^2\theta'$ prediction. We further compare the data with the Stodolsky-Sakurai Model by observing the N^* Treiman-Yang angular distribution. It is parametrized by the density matrix element $\mathrm{Re}\rho_{3-1}$ and has the general form:

$$W_{N^*}(\phi)\sim\left[\left(1-\frac{4}{\sqrt{3}}\mathrm{Re}\rho_{3-1}\right)+\frac{8}{\sqrt{3}}\mathrm{Re}\rho_{3-1}\sin^2\phi\right], \quad (15)$$

which is easily obtained from (10) by integrating over $\cos\theta$. The element $\mathrm{Re}\rho_{3-1}$ is predicted to be $0.216=\frac{3}{8}$ which leads to $W_{N^*}(\phi)1+2\sin^2\phi$ according to (15). The experimental value of $\mathrm{Re}\rho_{3-1}$ is 0.21 ± 0.03 which leads upon substitution in (15) to $W_{N^*}(\phi)=1+(1.9\pm0.5)\sin^2\phi$. It is shown normalized to the total number of N^* events in Fig. 12. This result is also in good agreement with the Stodolsky-Sakurai model and taken together with the result for the $\cos\theta'$ distribution indicates that $K^+p \to N^*K$ at this energy is consistent with meson exchange.

A comparison of the K^* and N^* density matrices corresponding to the reactions $K^+p \to K^*p$ and $K^+p \to N^*K$ with other experiments is made in Table III. For the K^* we note that with the exception of the 1.5 BeV/c experiment, the values of the parameter ρ_{00} are consistent. This may indicate the vector meson exchange plays an increasingly important part in this reaction as the energy increases. The values of ρ_{1-1} are also in fair agreement except at 5.0 BeV/c where an experimental value of 0.42 ± 11 is somewhat higher than our value of 0.24 ± 0.04. Finally, the values of $\mathrm{Re}\rho_{10}$ are also consistent with one another within experimental uncertainties. We have also included in Table III, the results of three K^-p experiments which represent the reaction $K^-p \to K^{*-}p \to \bar{K}^0\pi^-p$. This allows a comparison to be made with the K^+ experiments, particularly since two of the K^- experiments correspond in energy to two of the K^+ experiments. At 1.5 BeV/c the value of ρ_{00} is 0.40 ± 0.04 in K^+p and 0.38 in K^-p. These are in good agreement. However, the values of ρ_{00} in both charge states are larger at this energy than at higher energies indicating again that pseudoscalar exchange may be more important at lower energies. At

TABLE III. Variation of density matrices with energy.

K^* density matrix Inc. K^+ lab momentum (BeV/c)	ρ_{00}	ρ_{1-1}	$\mathrm{Re}\rho_{10}$	Reference
1.5	0.40 ± 0.04	...	...	6
2.26	0.15 ± 0.05	0.24 ± 0.04	-0.05 ± 0.03	...
3.0	0.07 ± 0.06	0.32 ± 0.06	-0.10 ± 0.05	9
5.0	0.25 ± 0.12	0.42 ± 0.11	-0.04 ± 0.09	18
$1.5K^-p$	0.38 ± 0.06	0.21 ± 0.06	...	a
$3.0K^-p$	0.17 ± 0.05	0.29 ± 0.04	0.01 ± 0.02	b
$3.5K^-p$	0.24 ± 0.06	0.19 ± 0.06	0.05 ± 0.04	c

N^* density matrix Inc. K^+ lab momentum (BeV/c)	ρ_{33}	$\mathrm{Re}\rho_{3-1}$	$\mathrm{Re}\rho_{31}$	Reference
2.26	0.28 ± 0.04	0.21 ± 0.03	-0.03 ± 0.04	...
3.0	0.28 ± 0.06	0.21 ± 0.05	0.04 ± 0.05	9

[a] S. L. Adelman, Report presented at *Proceedings of the Second Topical Conference on Resonant Particles, 1965* (University of Ohio, Athens, Ohio, 1965).
[b] R. Barloutaud, A. Leveque, C. Louedec, J. Meyer, P. Schlein, A. Verglas, J. Badier, M. Demoulis, J. Goldberg, B. P. Gregory, P. Krejbich, C. Pelletier, M. Ville, E. S. Gelsame, W. Hoagland, J. C. Kluyver, and A. G. Tenner, Phys. Rev. Letters 12, 352 (1964).
[c] N. Haque, Rutherford Laboratory, Cambridge, Report No. RPP/H/3, 1965 (unpublished).

3.0-BeV/c values of all three ρ parameters are available in both charge states. With the exception of the element $\mathrm{Re}\rho_{10}$, the values of the density matrix elements are consistent with each other at this energy.

For the channel $K^+p \to N^*K$ we compare our results with those of the CERN group.[9] The agreement between the two sets of N^* density matrix elements is very good.

5. DIFFERENTIAL PRODUCTION CROSS SECTIONS OF THE RESONANCES

We described in the previous section an analysis of the decay correlations which leads us to conclude that the production of the K^* and N^* resonances in our experiment is consistent with a mixture of pseudoscalar and vector meson exchange with the latter predominating. In this section we analyze the differential production cross sections of the resonances, assuming that these exchange processes are responsible for the channels $K^+p \to K^*p$ and $K^*p \to N^*K$. We shall see that the agreement between our data and the theoretical predictions is only moderate.

Theoretical expressions for these cross sections have been worked out by Jackson and Gottfried.[16–18] They have included in this theory, absorptive modifications to the simple peripheral model. They begin with a general expression[13] for the differential cross section for a reaction $a+b \to c+d$:

$$\frac{d\sigma}{d\Omega}=\frac{1}{(2S_a+1)(2S_b+1)}\frac{q'}{sq}\sum_{\lambda_a\lambda_b\lambda_c\lambda_d}|\langle\lambda_c\lambda_d|T|\lambda_a\lambda_b\rangle|^2, \quad (16)$$

where q and q' are the initial and final center-of-mass three-momenta, s is the square of the total center-of-mass energy, T is the transition operator which describes the production of c and d from a and b and the right-hand side of (16) is averaged over initial and summed over final-state helicities. We note that the T operator appropriate to the present case is a single-meson exchange operator. Upon substituting explicit expressions for the T operators[13] and adding amplitudes for pseudoscalar and vector meson exchange, the predictions of the simple peripheral model are obtained. As we noted before, in this simple model the pseudoscalar and vector exchange amplitudes add incoherently. Jackson and Gottfried[16–18] pointed out, however, that (16) as it stands cannot be correct for a single-particle-exchange process. The essence of their remarks is that a sum over all possible orbital angular momenta in the initial state is implied in (16). This is unreasonable because we expect peripheral collisions or single-particle-exchange processes to occur in high orbital-angular-momentum states, or alternatively when the initial-state impact parameter is fairly large. We expect that in an almost head on collision the probability for single-particle exchange is very small. It is therefore necessary to modify (16) so that the contributions from the low orbital-angular-momentum states is reduced. The prescription for carrying out this reduction is based on the assumption[16–18] that if the energy in the initial state is high enough, the interactions which compete strongly with single-particle exchange in low orbital states can be taken to be elastic scattering interactions between the initial particles a, b and between the final particles c, d. These elastic scattering interactions are expressed in terms of the small-angle differential cross sections (as a function of four-momentum transfer) as[16–18]

$$(d\sigma/dt)=\frac{\sigma_{\mathrm{total}}^2}{16\pi^2}e^{-At}, \quad (17)$$

where t is the four-momentum transfer and A is a constant. Furthermore, it is shown in Refs. 16–18, that the elastic-scattering phase shifts can be written as

$$e^{2i\delta(b)}=1-\frac{\sigma_{\mathrm{total}}}{4\pi A}e^{-b^2/2A}, \quad (18)$$

where the impact parameter b is related to the orbital angular momentum l, by

$$l=qb. \quad (19)$$

Here q is the linear momentum of either of the colliding particles in their center-of-mass system. To modify the single-particle-exchange amplitudes, one first expands them in a series of partial waves:

$$\langle\lambda_c\lambda_d|T|\lambda_a\lambda_b\rangle=\textstyle\sum_j(j+\frac{1}{2})\langle\lambda_c\lambda_d|T^j|\lambda_a\lambda_b\rangle d_{\lambda\mu}{}^j. \quad (20)$$

This expression is due to Jacob and Wick.[21] Here λ_a, λ_b, λ_c, and λ_d are as before the helicities of the initial and final particles, $\lambda=\lambda_a-\lambda_b$, $\mu=\lambda_c-\lambda_d$, j is the total angular momentum and $d_{\lambda\mu}{}^j(\theta)$ are $(2j+1)$ dimensional representations of the rotation group. Jackson and Gottfried's prescription for modifying the partial-wave components of each helicity amplitude is this: Each component is multiplied by an elastic-scattering phase shift appropriate to initial-state scattering, and by a similar phase shift appropriate to final-state scattering. It is convenient in discussing the ensuing expressions to express the partial-wave expansion as an integral rather than a sum, with the discrete variable j of (20) being replaced by a continuous variable x. The jth partial-wave component of the helicity amplitude is then written as $\langle\lambda_c\lambda_d|T(x)|\lambda_a\lambda_b\rangle$ and the phase shifts (18) can also be expressed in terms of x. Then the modified-partial-wave component is

$$\langle\lambda_c\lambda_d|T^M(x)|\lambda_a\lambda_b\rangle = e^{i\delta_{cd}(x)}\langle\lambda_c\lambda_d|T(x)|\lambda_a\lambda_b\rangle e^{i\delta_{ab}(x)}. \quad (21)$$

The phase shifts can be expressed, similarly to Eq. (18), as:

$$e^{i\delta_{ab}(x)}=(1-C_1e^{-\gamma_1x^2})^{1/2}, \qquad e^{i\delta_{cd}(x)}=(1-C_2e^{-\gamma_2x^2})^{1/2}. \quad (22)$$

In (22) C_1 and C_2 are measures of the amounts by which

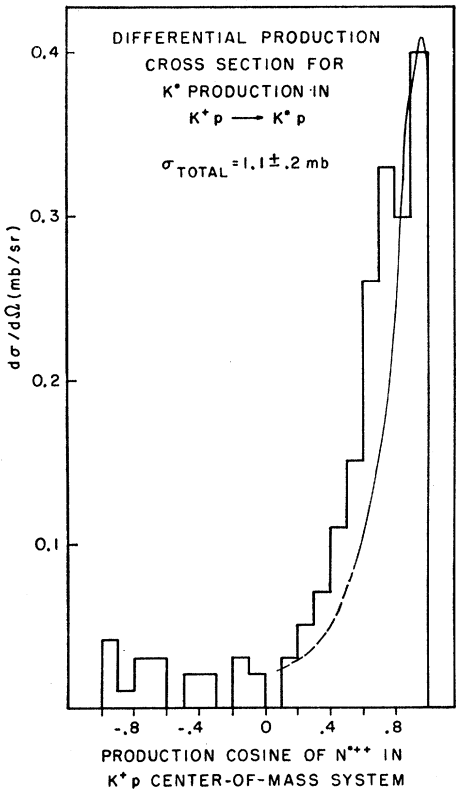

FIG. 13. Differential production cross section of K^* versus $\cos\theta_{\text{c.m.}}^{K^*}$, where $\cos\theta_{\text{c.m.}}^{K^*}=\hat{K}_{\text{beam}}^{+}\cdot\hat{K}^*$.

the lowest partial waves are absorbed in the initial and final states and γ_1 and γ_2 are proportional to $(1/A_1)$ and $(1/A_2)$. From the differential scattering cross section (17), A_1 and A_2 are constants which measure the slopes of the elastic cross sections at small angles or low four-momentum transfers. We remark, following Jackson and Gottfried, that C_1 and γ_1 are generally associated with the elastic scattering of one or two dynamically unstable particles and are not known. Therefore, a reasonable assumption about their values must be made in any experiment. Furthermore, because of the reduction factors occurring in the partial-wave expansions of the helicity amplitudes, the pseudoscalar and vector exchange amplitudes no longer add incoherently as in the simple peripheral model.

Gottfried, Jackson, and Svennson[18] used the theory outlined above to fit the differential cross sections of the K^* and N^* obtained in the CERN 3.0-BeV/c K^+p experiment. For the reaction $K^+p\to K^{*+}p$ in which both pseudoscalar and vector meson exchange are allowed, a mixture of pion and vector meson exchange was taken, with the mass of the vector meson equal to 750 MeV. The best fit to the data of that experiment[9] was obtained by varying the ratios of vector to pseudoscalar coupling constants. These ratios are denoted[18] by

$$\xi=\frac{f_{\pi K^*V}(G_{Vp\bar{p}}{}^{V}+G_{Vp\bar{p}}{}^{T})}{2g_{\pi\pi K^*}G_{\pi p\bar{p}}},$$

$$\eta=\frac{f_{\pi K^*V}G_{Vp\bar{p}}{}^{T}}{g_{\pi\pi K^*}G_{\pi p\bar{p}}}.$$

Using the values of ξ and η which gave good fits to the data at 3.0 BeV/c, Jackson and co-workers at the University of Illinois calculated a series of theoretical differential cross sections for the K^* in $K^+p\to K^*p\to K^0\pi^+p$ at the present energy. We may thus use our data to see if a given pair of ratios, ξ, η, gives agreement at 2.26 BeV/c and 3.0 BeV/c. That pair of parameters which gives best agreement with our data is $\xi=1.55$ and $\eta=1.48$. The remaining absorptive parameters for this theoretical curve are

$$C_1=1.00,\quad C_2=1.00,$$
$$\gamma_1=0.21,\quad \gamma_2=0.16.$$

We compare our experimental differential cross section for the K^* with this theoretical curve in Fig. 13. The histogram, as usual, represents the experiment and the solid curve is the theoretical prediction. The two agree

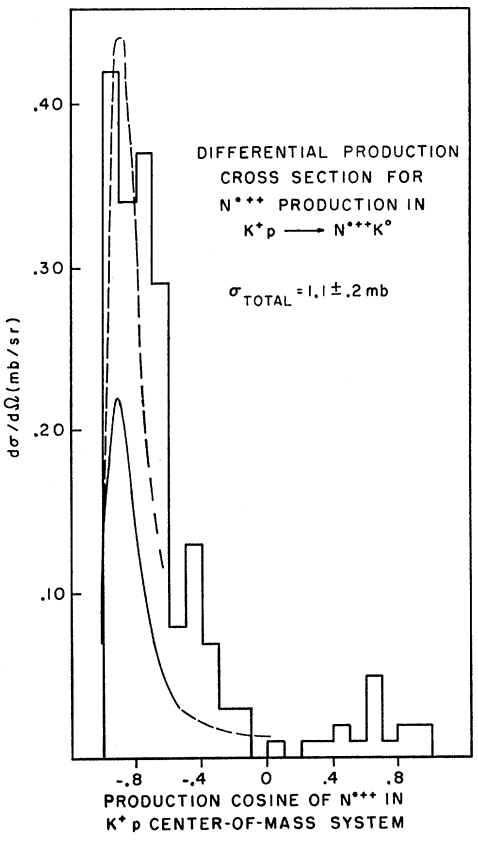

FIG. 14. Differential production cross section of N^* versus $\cos\theta_{\text{c.m.}}^{N^*}=\hat{K}_{\text{beam}}^{+}\cdot\hat{N}^*$.

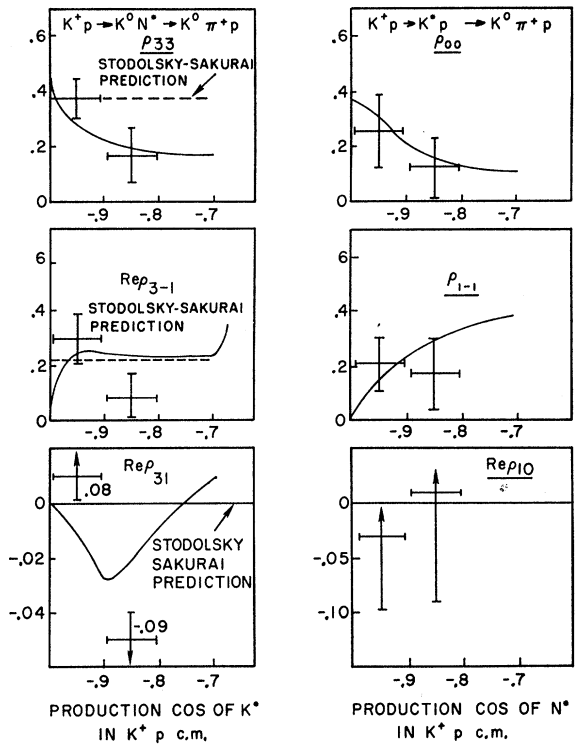

FIG. 15. Variation of density matrix elements of K^* and N^* with center-of-mass production angle ($\cos\theta_{\text{c.m.}}^{K^*}$ or $\cos\theta_{\text{c.m.}}^{N^*}$).

reasonably well particularly at very small production angles, say $\cos\theta > 0.85$.

Jackson has also calculated a theoretical differential cross section for the reaction $K^+p \to N^*K \to K^0\pi^+p$ at 2.26 BeV/c. In this reaction pseudoscalar exchange is not allowed and only ρ meson exchange was considered in accordance with the Stodolsky-Sakurai Model. The ρ meson coupling constants were chosen in conformity with this model and such that $g_{K^+\rho K^0}G_{p\rho N^*} = 50 \times 16\pi^2$. The remaining absorptive parameters used in the calculation were

$$C_1 = 1.0, \quad C_2 = 1.0,$$
$$\gamma_1 = 0.17, \quad \gamma_2 = 0.085.$$

The experimental cross section is compared with the theory in Fig. 14. The agreement in this case is not very good. The dashed curve represents the predicted cross section normalized to the point at $\cos\theta = 1$. We have performed this renormalization only for an easy comparison of the shapes of the theoretical and experimental differential cross sections. We remark from Fig. 14 that the shapes are in fair agreement for very backward N^*'s with $\cos\theta < -0.8$.

We note[16–18] that a peripheral model with absorption predicts that the density matrix elements of a resonance should vary with its production angle. We calculate the K^* and N^* density matrices over the production cosine ranges 0.9, 1.0 and 0.8, 0.9 for the K^* and -1.0, -0.9 and -0.9, -0.8 for the N^*. The experimental results are compared with the theory in Fig. 15.

6. CONCLUSION

For the reaction $K^+p \to K^0\pi^+p$ at 2.26 BeV/c we find a cross section of 2.62 ± 0.30 mb with production of each of the K^* and N^* resonances occurring about 40% of the time. The intrinsic masses and widths of these resonances determined in this experiment are $M_{K^*} = 895 \pm 3$ MeV, $\Gamma_{K^*} = 50 \pm 5$ MeV, $M_{N^*} = 1234 \pm 5$ MeV, and $\Gamma_{N^*} = 120 \pm 30$ MeV. These agree with the values of these parameters determined from similar data at 3.0 BeV/c.

Analysis of the decay angular distributions of the resonances indicates consistency of the data with a single-particle-exchange model. Vector meson exchange seems to be the predominating production mechanism for both the K^* and N^*. In particular for the latter of these, the reaction $K^+p \to N^*K$ is in good agreement with the Stodolsky-Sakurai model as far as the N^* decay correlations are concerned. For the K^*, the nonzero value of the density matrix element $\text{Re}\rho_{10}$ indicates a lack of agreement with a simple peripheral model.

When the differential cross sections for the production of these resonances are compared with the predictions of a pheripheral model modified to account for absorptive effects there is at best moderate agreement.

ACKNOWLEDGMENTS

We would like to express our gratitude to the operating crew of the 20-in. hydrogen bubble chamber and the A.G.S. staff at Brookhaven National Laboratory for their cooperation and help during the exposure. We are also indebted to Professor Gordon Kane for many invaluable discussions and to Professor J. D. Jackson and his colleagues for calculating the theoretical differential cross-section curves for us. We also wish to thank the scanning and measuring staff at Johns Hopkins for their excellent work during the analysis of the photographs.